DEVELOPMENT OF FLUID-SEDIMENT-SEABED INTERACTION MODEL AND ITS APPLICATION

Tomoaki Nakamura[1] and Norimi Mizutani[1]

To provide a computational framework for simulating fluid-sediment-seabed interactions, a three-dimensional coupled fluid-sediment-seabed interaction model was developed and applied to seabed response under regular waves and local scouring from tsunami run-up. For the seabed response under the regular waves, the validity of the model was verified from comparison with an analytical solution. For the seabed response under the tsunami-induced local scouring, numerical results showed that the model had sufficient computational capability to simulate the seabed response during the onset of the local scouring, and suggested that the model is a useful tool for analyzing and evaluating a general complex fluid-sediment-seabed interaction phenomenon in a marine environment.

Keywords: fluid-sediment-seabed interaction; numerical model; finite element method; coupling scheme; tsunami-induced local scouring

INTRODUCTION

Complex multi-physics fields formed by dynamic interactions between fluid flows, seabed profile evolution, and seabed response are natural in a marine environment. Modeling of such fluid-sediment-seabed interactions is essential to accurately simulate and analyze spatial and temporal change in the surface profile of the seabed and resulting response of the seabed under wave action. To deal with this type of interaction phenomenon, numerical models applicable to fluid-sediment interaction (e.g., Lee and Mizutani 2006, Liu and García 2008, Nakamura and Yim 2011) and those applicable to fluid-seabed interaction (e.g., Jiang et al. 2000, Takahashi et al. 2002, Nakamura et al. 2008) have been developed independently. However, no analytical and numerical tools which consider the physics of the entire coupled fluid-sediment-seabed system are currently available.

To provide an overarching computational framework for simulating fluid-sediment-seabed interactions, a three-dimensional coupled fluid-sediment-seabed interaction model and a corresponding numerical code are developed in this study. To verify the validity of the model, it is applied to seabed response under regular waves. To demonstrate the computational capability of the model, it is also applied to hydraulic experiments on tsunami-induced local scouring.

THREE-DIMENSIONAL COUPLED FLUID-SEDIMENT-SEABED INTERACTION MODEL

The three-dimensional coupled fluid-sediment-seabed interaction model is composed of a main solver and three modules. The main solver is a large-eddy simulation model based on continuity and momentum equations for incompressible viscous air-water multi-phase flow that considers seepage flow in porous media and the profile evolution of a sediment bed. The first module is a volume-of-fluid (VOF) module based on the multi-interface advection and reconstruction solver (MARS; Kunugi 2000) for air-water interface tracking. The second module is a sediment transport (ST) module for computing the surface profile evolution of a sediment bed induced by bed-load and suspended sediment transport, and the distribution of suspended sediment concentration that considers all transport processes of pickup, advection, diffusion, and settling. The third module is a finite element (FE) module based on a finite element method computing the *u-p* approximation of the Biot equation for coupled soil-water analysis of the sediment bed. In the following sections, the FE module and a coupling procedure between the main solver and the modules are presented in detail. Explanations of the main solver and the VOF and ST modules can be found in Nakamura and Yim (2011).

Finite Element Module

In this module, the following *u-p* approximation of the Biot equation, which is derived from the complete form of the Biot equation assuming that the acceleration of relative water displacement $\ddot{w}_i$ is smaller than that of soil skeleton $\ddot{u}_i$, is used after Takahashi et al. (2002):

$$\rho\ddot{u}_i = -\sigma'_{ji,j} - p_{,i} + \rho g_i \tag{1}$$

$$-\frac{\partial \varepsilon_{kk}}{\partial t} + \frac{m}{K_w}\dot{p} + \left\{ \frac{k_s}{\rho_w g}\left(-\rho_w \ddot{u}_i - p_{,i} + \rho_w g_i\right) \right\}_{,i} = 0 \tag{2}$$

[1] Department of Civil Engineering, Nagoya University, Furo-cho, Nagoya 464-8603, Japan

where u_i is the displacement vector of soil skeleton; p is the pore-water pressure; σ'_{ij} is the effective stress tensor, which is defined as positive in compression; ε_{ij} is the strain tensor; x_i is the position vector; t is the time; m is the porosity of soil; ρ is the density of soil (= $(1 - m)\rho_s + m\rho_w$); ρ_s is the density of soil particles; ρ_w is the density of water; k_s is the hydraulic conductivity of soil; K_w is the apparent bulk modulus of water; g_i is the vector of the gravitational acceleration (= $[0\ 0\ -g]^{\mathrm{T}}$); and g is the gravitational acceleration. As a constitutive equation, the following Hooke law for isotropic elastic materials nonresistant to tensile force is adopted for simplicity:

$$\sigma'_{ij} = \lambda\varepsilon_{kk}\delta_{ij} + 2\mu\varepsilon_{ij} \tag{3}$$

in which λ and μ are the Lamé constants, which are given as

$$\lambda = \frac{E\nu}{(1+\nu)(1-2\nu)} \tag{4}$$

$$\mu = \frac{E}{2(1+\nu)} = G \tag{5}$$

under compression, and $\lambda = \mu = 0$ under tension. In these equations, E is the modulus of elasticity, G is the shear modulus of elasticity, and ν is the Poisson ratio.

After Sandhu's formulation (e.g., Sandhu and Wilson 1969), the incremental form of the finite element equation is derived as

$$\begin{bmatrix} \mathbf{M}^{UU} & \mathbf{0} \\ \mathbf{M}^{PU} & \mathbf{0} \end{bmatrix}\begin{bmatrix} d\ddot{\mathbf{U}} \\ d\ddot{\mathbf{P}} \end{bmatrix} + \begin{bmatrix} \mathbf{0} & \mathbf{0} \\ \mathbf{C}^{PU} & \mathbf{C}^{PP} \end{bmatrix}\begin{bmatrix} d\dot{\mathbf{U}} \\ d\dot{\mathbf{P}} \end{bmatrix} + \begin{bmatrix} \mathbf{K}^{UU} & -\mathbf{K}^{UP} \\ \mathbf{0} & \mathbf{K}^{PP} \end{bmatrix}\begin{bmatrix} d\mathbf{U} \\ d\mathbf{P} \end{bmatrix} = \begin{bmatrix} d\mathbf{F} \\ -d\mathbf{Q} \end{bmatrix} \tag{6}$$

from Eqs. (1) and (2), and computed using a finite element method. In this equation, $d\mathbf{U}$ and $d\mathbf{P}$ are the incremental forms of the global soil displacement vector $\mathbf{U}$ and pore-water pressure vector $\mathbf{P}$, and $\mathbf{M}^{UU}$, $\mathbf{M}^{PU}$, $\mathbf{C}^{PU}$, $\mathbf{C}^{PP}$, $\mathbf{K}^{UU}$, $\mathbf{K}^{UP}$, $\mathbf{K}^{PP}$, $d\mathbf{F}$, and $d\mathbf{Q}$ are written as

$$\mathbf{M}^{UU} = \int_\Omega \mathbf{N}^{\mathrm{T}}\rho\mathbf{N}\, dv \tag{7}$$

$$\mathbf{M}^{PU} = \int_\Omega \mathbf{G}^{\mathrm{T}}\frac{k_s}{g}\mathbf{N}\, dv \tag{8}$$

$$\mathbf{C}^{PU} = \int_\Omega \bar{\mathbf{N}}^{\mathrm{T}}\mathbf{m}^{\mathrm{T}}\mathbf{B}\, dv \tag{9}$$

$$\mathbf{C}^{PP} = \int_\Omega \bar{\mathbf{N}}^{\mathrm{T}}\frac{m}{K_w}\bar{\mathbf{N}}\, dv \tag{10}$$

$$\mathbf{K}^{UU} = \int_\Omega \mathbf{B}^{\mathrm{T}}\mathbf{D}\mathbf{B}\, dv \tag{11}$$

$$\mathbf{K}^{UP} = \int_\Omega \mathbf{B}^{\mathrm{T}}\mathbf{m}\bar{\mathbf{N}}\, dv \tag{12}$$

$$\mathbf{K}^{PP} = \int_\Omega \mathbf{G}^{\mathrm{T}}\frac{k_s}{\rho_w g}\mathbf{G}\, dv \tag{13}$$

$$d\mathbf{F} = \int_{\partial\Omega_t} \mathbf{N}^{\mathrm{T}} d\hat{\mathbf{t}}\, ds \tag{14}$$

$$d\mathbf{Q} = \int_{\partial\Omega_q} \bar{\mathbf{N}}^{\mathrm{T}} d\hat{\mathbf{q}}\, ds \tag{15}$$

in which $\mathbf{N}$ and $\bar{\mathbf{N}}$ are the shape functions of $d\mathbf{U}$ and $d\mathbf{P}$; $\mathbf{D}$ is the stress-strain matrix; $\mathbf{B}$ is the displacement-strain matrix (= $\mathbf{L}\mathbf{N}$); $\mathbf{G} = \bar{\mathbf{L}}\bar{\mathbf{N}}$; $d\hat{\mathbf{t}}$ is the incremental form of external force vector on a unit area of the traction boundary $\partial\Omega_t$; $d\hat{\mathbf{q}}$ is the incremental form of water discharge on the natural boundary $\partial\Omega_q$; $\mathbf{m}$ is the vector notation of Kronecker's delta δ_{ij}; and $\mathbf{L}$ and $\bar{\mathbf{L}}$ are the matrix and vector notations of the Laplace operator ∇. For stable computation of the spatial discretization, the twenty-node quadratic and eight-node linear isoparametric brick elements were used as $\mathbf{N}$ and $\bar{\mathbf{N}}$. For the time integration, the Newmark β and Crank-Nicolson schemes were adopted for $d\mathbf{U}$ and $d\mathbf{P}$. In addition, the modified Newton-Raphson scheme was used for the nonlinear constitutive equation.

Coupling Procedure

In the model, the VOF and ST modules are connected to the main solver using a two-way coupling procedure implemented at every time step to ensure fluid-sediment interaction. To ensure the continuity of seepage flow velocity and pore-water pressure on the surface of a sediment bed, the FE module is connected to the main solver using a one-way coupling procedure proposed by Mizutani et

al. (1996). To take into account the surface profile evolution of the bed induced by sediment transport, the FE module is also connected to the ST module using a same procedure as the simulation of embankment construction and excavation. Specifically, node force equivalent to the weight of added elements acts downward for deposition, while node force equivalent to the weight of deleted elements acts upward for erosion. Figure 1 shows the coupling procedure, which is implemented as follows:

1. The flow velocity v_i^n and pressure p^n at the nth time step are computed using the main solver.
2. The VOF function F^n is computed using the VOF module.
3. The suspended sediment concentration C^n and the height of the surface of the sediment bed above a reference level z_s^n are computed using the ST module.
4. The seepage flow velocity and pore-water pressure on the surface of the bed are interpolated from v_i^n and p^n, and the values of $d\mathbf{U}^n$ and $d\mathbf{P}^n$ are computed using the FE module.
5. The main module is implemented again to compute the values of v_i^{n+1} and p^{n+1} at the next (n + 1)th time step from v_i^n, p^n, F^n, and z_s^n.
6. This procedure is repeated until the value of n reaches the number of specific time steps.

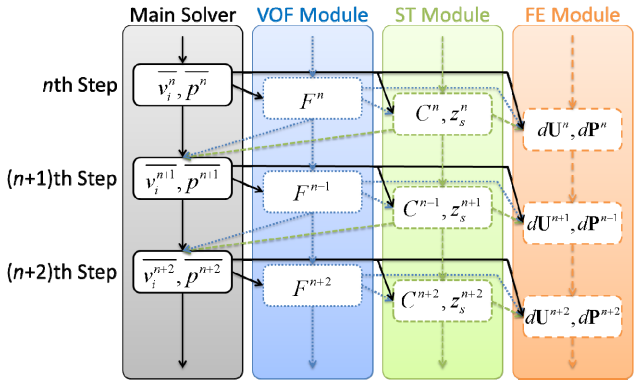

Figure 1. Coupling procedure.

SEABED RESPONSE UNDER REGULAR WAVES

Dynamic response of the seabed under regular waves was computed and compared with an analytical solution derived by Yamamoto (1977). Figure 2 shows a schematic of a computational domain. As shown in this figure, the horizontal flat seabed was set in a pit with a length of 6.0 m and a depth of 0.3 m, and regular waves with a period T of 1.0 s, a height H_i of 0.03 m at the center of the seabed (x = 5.0 m), and a still water depth h of 0.3 m were generated. The values of the median grain size of soil particles d_{50}, porosity of the seabed m, density of the soil particles ρ_s, shear modulus of elasticity G, and Poisson ratio ν were set at 0.45 mm, 0.4, 2.65×10^3 kg/m^3, 10^8 N/m^2, and 0.33, and the hydraulic conductivity of the seabed k_s was determined from the following equations (Bear 1972):

$$k_s = \frac{1}{180}\frac{m^3}{(1-m)^2}\frac{gd_{50}^2}{\nu_w} \tag{16}$$

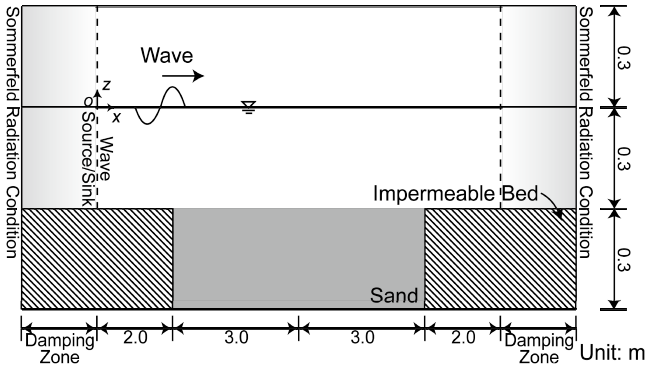

Figure 2. Computational domain for the seabed response under the regular waves.

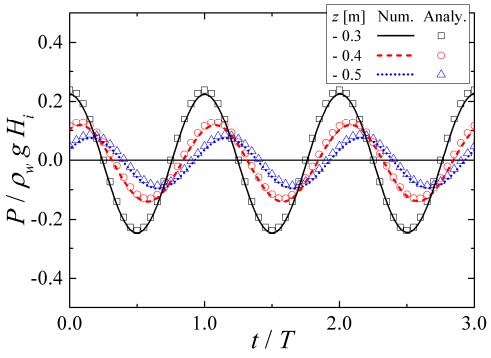

(a) Pore-water pressure *P*.

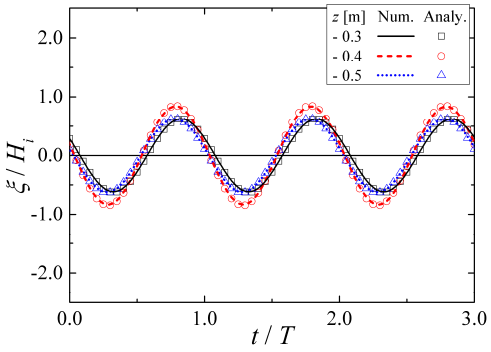

(b) Horizontal displacement *ξ*.

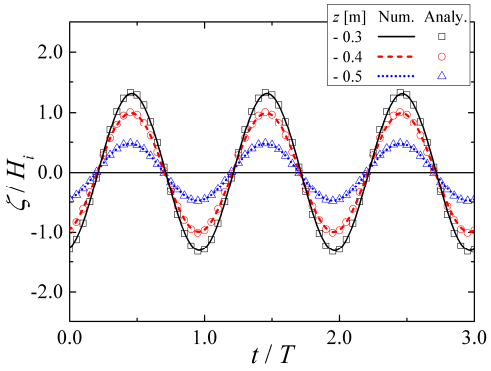

(c) Vertical displacement *ζ*.

Figure 3. Comparison with the analytical solution for K_w = 2.2×10^5 N/m^2.

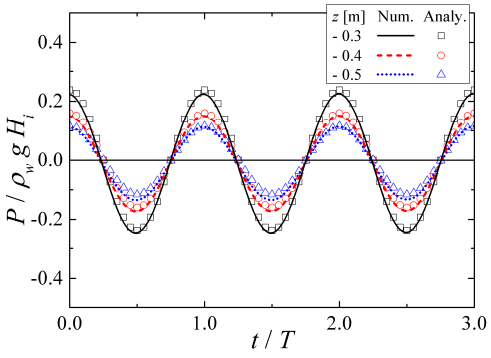

(a) Pore-water pressure *P*.

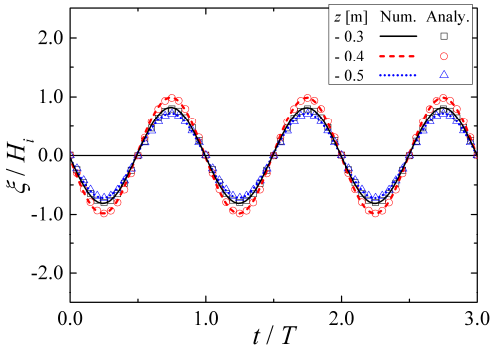

(b) Horizontal displacement *ξ*.

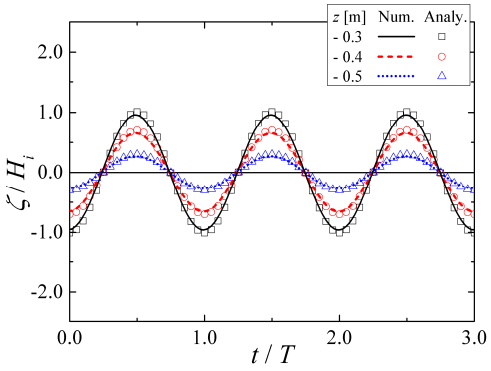

(c) Vertical displacement *ζ*.

Figure 4. Comparison with the analytical solution for K_w = 2.2×10^7 N/m^2.

in which ν_w is the kinematic molecular viscosity of water. The apparent bulk modulus of water K_w was changed to 2.2×10^5 N/m^2 and 2.2×10^7 N/m^2. The other parameters were the same as Nakamura and Yim (2011). Note that the ST module were not used because it was assumed in Yamamoto (1977) that the surface profile of the seabed did not change.

Figures 3 and 4 show a comparison of pore-water pressure P, horizontal displacement of the seabed skeleton ξ, and vertical displacement of the seabed skeleton ζ at the center of the seabed (x = 5.0 m). As shown in these figures, the amplitudes of P and ζ decrease in the negative z direction, while that of ξ at z = –0.4 m is larger than that near the surface and bottom of the seabed. Furthermore, the phase of P gradually delays in the negative z direction for K_w = 2.2×10^5 N/m^2 unlike K_w = 2.2×10^7 N/m^2. From Figs. 3 and 4, it is also found that the numerical results are consistent with the analytical solution in terms of the attenuation and phase of P and the damping of ξ and ζ.

As a result, it was demonstrated that the validity of the FE module and the coupling procedure was verified against the analytical solution.

SEABED RESPONSE UNDER TSUNAMI-INDUCED LOCAL SCOURING

Computational Domain and Condition

To examine the computational capability of the model, it was applied to hydraulic experiments on tsunami-induced local scouring around an inland structure (Nakamura et al. 2008). Figure 5 shows a schematic of a computational domain modeled from a 1/20 scale experimental setup. As shown in this figure, an impermeable seawall and a sand substrate with a median grain size d_{50} of 0.2 mm were set on an impermeable bed, and an impermeable structure with a 0.14-m-wide square cross-section was fixed at 0.28 m landward from the landward surface of the seawall. Because of the lack of available experimental data, the values of the porosity of the substrate m, density of sand particles ρ_s, shear modulus of elasticity G, Poisson ratio ν, and apparent bulk modulus of water K_w were assumed to be 0.4, 2.65×10^3 kg/m^3, 10^8 N/m^2, 0.33, and 2.2×10^7 N/m^2, and the hydraulic conductivity k_s was estimated to be 4.34×10^{-4} m/s from Eq. (16). The other parameters were the same as the previous section.

In this study, a representative wave condition was selected from over 150 cases in the hydraulic experiments. The still water depth h was set at 0.455 m, and a single leading long-period wave with a duration of 6.0 s and a height of 0.064 m at W1 (see Fig. 5) was generated toward the substrate.

Note that the computational accuracy of the main solver, VOF module, and ST module was confirmed against experimental data in terms of water surface elevation, pore-water pressure, and final surface profile of the substrate. For details, see Nakamura and Mizutani (2012).

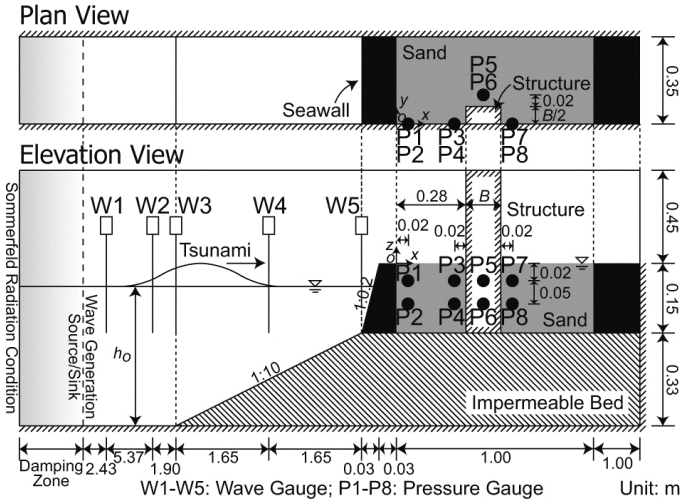

Figure 5. Computational domain for the seabed response during the onset of the tsunami-induced local scouring.

Numerical Results and Discussion

Figures 6, 7, and 8 show pore-water pressure P, mean effective stress σ'_m and relative effective stress ratio γ (RESR; $= 1-\sigma'_m / \sigma'_{m0}$; σ'_{m0} : initial value of σ'_m), in which the γ value is one of the non-dimensional indices for evaluating liquefaction, with liquefaction occurring when $\gamma = 1$.

From Figs. 6(a) and 7(a), at which the run-up tsunami begins to touch the seaward surface of the structure, it is observed that the value of P increases and that of σ'_m decreases near the surface of the substrate at the landward side of the seawall. This decrease in σ'_m, as shown in Fig. 8(a), causes an increase in γ, suggesting the onset of liquefaction. Conversely, the value of γ decreases at the seaward side of the structure because of an increase in σ'_m . After that, as indicated in Fig. 6(b), the value of P increases near the surface of the substrate at the seaward side of the structure. However, around the seaward corner of the structure, the P value remains close to zero and the load on the substrate decreases due to local scouring, resulting in a decrease in σ'_m and a resultant increase in γ (see Figs. 7(b) and 8(b)). This result suggests that liquefaction occurs during the local scouring. Similar phenomenon was observed in Tonkin et al. (2003). After the tsunami subsides, as shown in Figs. 6(c), 7(c), and 8(c), it is observed that although the value of P returns to zero, the γ value remains high.

From these results, it is found that the model has sufficient computational capability for assessing dynamic response of a sediment bed during the onset of tsunami-induced local scouring. This also

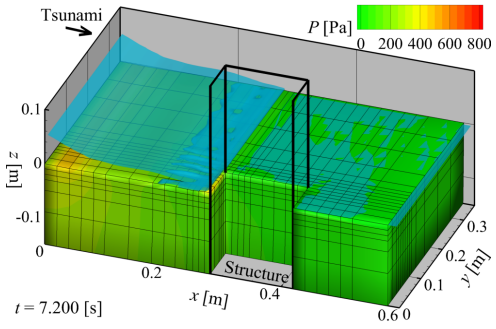

(a) t = 7.2 s.

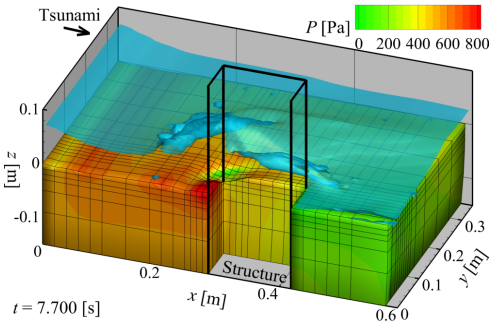

(b) t = 7.7 s.

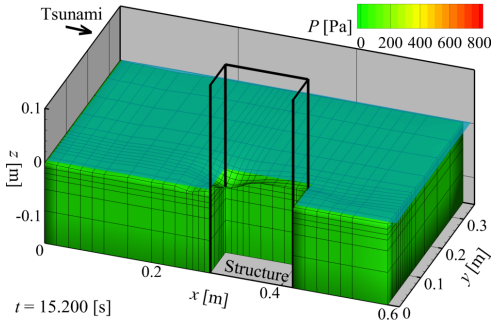

(c) t = 15.2 s.

Figure 6. Distribution of the pore-water pressure *P*.

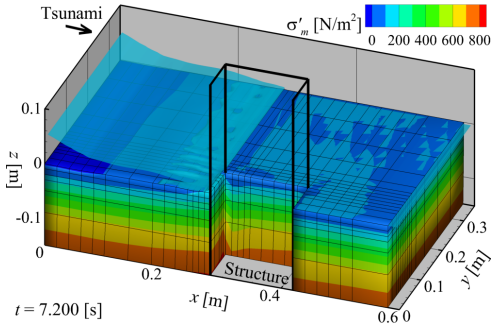

(a) t = 7.2 s.

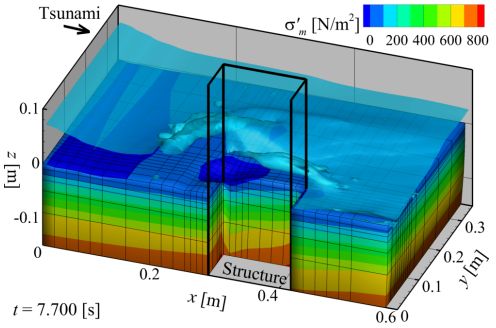

(b) t = 7.7 s.

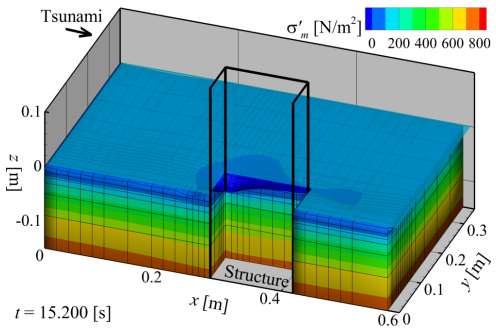

(c) t = 15.2 s.

Figure 7. Distribution of the mean effective stress σ'_m .

suggests that the model is a useful tool for analyzing and evaluating a general complex fluid-sediment-seabed interaction phenomenon in a marine environment.

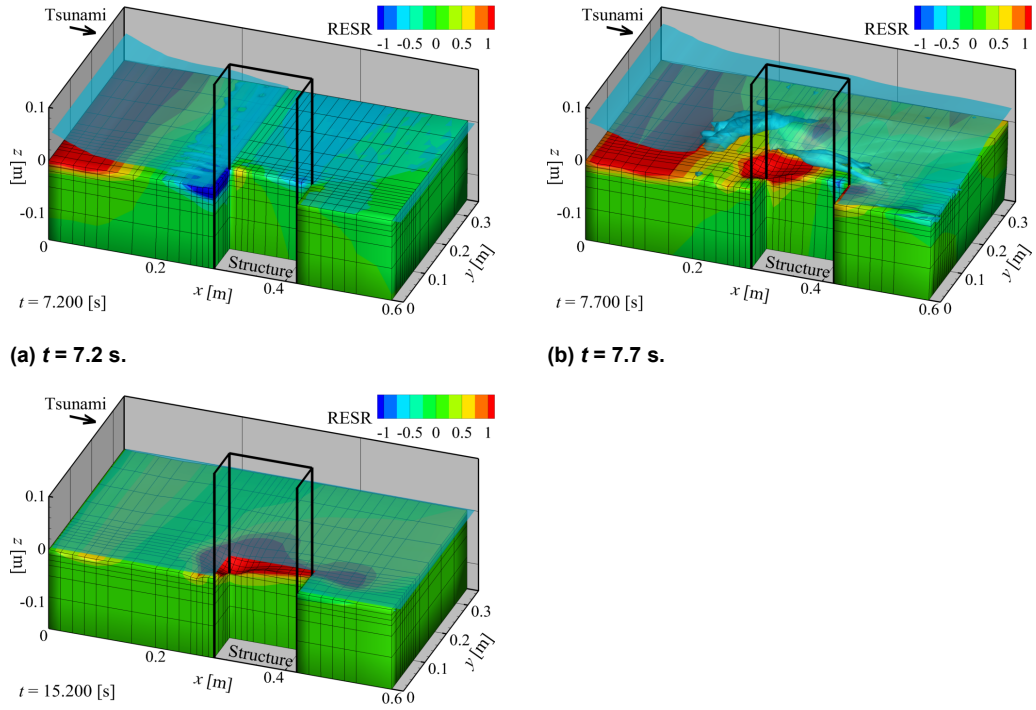

(a) *t* = 7.2 s. **(b) *t* = 7.7 s.**

(c) *t* = 15.2 s.

Figure 8. Distribution of the relative effective stress ratio (RESR) γ.

CONCLUDING REMARKS

A three-dimensional fluid-sediment-seabed interaction model that consistently considered the physics of the entire coupled fluid-sediment-seabed system was developed and applied to seabed response under regular waves and local scouring from tsunami run-up. The model is composed of a main solver based on a large-eddy simulation model for incompressible viscous air-water multi-phase flow, a volume-of-fluid module for air-water interface tracking, a sediment transport module for computing the surface profile of a sediment bed and suspended sediment concentration, and a finite element module for coupled soil-water analysis of the bed. The three modules were connected to the main solver using a coupling procedure that ensured fluid-sediment-seabed interactions.

For the seabed response under the regular waves, it was found that the validity of the finite element module and the coupling procedure was verified from comparison with an analytical solution in terms of pore-water pressure and displacement of the seabed skeleton. For the seabed response under the tsunami-induced local scouring, it was found that the model had sufficient computational capability to simulate pore-water pressure, mean effective stress, and relative effective stress ratio during the onset of the local scouring. From these results, it was confirmed that the model is a useful tool for analyzing and evaluating a general complex fluid-sediment-seabed interaction phenomenon in a marine environment.

ACKNOWLEDGMENTS

This research was partly supported by the Japanese Ministry of Land, Infrastructure, Transport and Tourism under the Research and Development of River and Sediment Control Technology (Coastal Technology Field; principal investigator: Norimi Mizutani).

REFERENCES

Bear, J. 1972. *Dynamics of Fluids in Porous Media*, American Elsevier Pub. Co., New York, 764 p.

Jiang, Q., S. Takahashi, Y. Muranishi, and M. Isobe. 2000. A VOF-FEM model for the interaction among waves, soils and structures, *Proceedings of Coastal Engineering*, JSCE, 47, 51-55 (in Japanese).

Kunugi, T. 2000. MARS for multiphase calculation, *Computational Fluid Dynamics Journal*, 9(1), 1-10.

Lee, K. H., and N. Mizutani. 2006. Local scour near a vertical submerged breakwater and development of its time domain analysis, *Annual Journal of Coastal Engineering*, JSCE, 53, 501-505 (in Japanese).

Liu, X., and M. H. García. 2008. Three-dimensional numerical model with free water surface and mesh deformation for local sediment scour, *Journal of Waterway, Port, Coastal, and Ocean Engineering*, ASCE, 134(4), 203-217.

Mizutani, N., W. G. McDougal, and A. M. Mostafa. 1996. BEM-FEM combined analysis of nonlinear interaction between wave and submerged breakwater, *Proceedings of 25th International Conference on Coastal Engineering*, ASCE, Orlando, FL, 2377-2390.

Nakamura, T., Y. Kuramitsu, and N. Mizutani. 2008. Tsunami scour around a square structure, *Coastal Engineering Journal*, JSCE, 50(2), 209-246.

Nakamura, T., and S. C. Yim. 2011. A nonlinear three-dimensional coupled fluid-sediment interaction model for large seabed deformation, *Journal of Offshore Mechanics and Arctic Engineering*, ASME, 133(3), 031103-1-031103-14.

Nakamura, T., and N. Mizutani. 2012. Sediment transport model considering pore-water pressure in surface layer of seabed and its application to local scouring due to tsunami, *Journal of Japan Society of Civil Engineers, Series B2 (Coastal Engineering)*, JSCE, 68(2), I_216-I_220 (in Japanese).

Sandhu, R. S., and E. L. Wilson. 1969. Finite element analysis of seepage in elastic media, *Journal of the Engineering Mechanics Division*, ASCE, 95, EM3, 641-652.

Takahashi, S., K. Suzuki, Y. Muranishi, and M. Isobe. 2002. U-π form VOF-FEM program simulating wave-soil interaction: CADMAS-GEO-SURF, *Proceedings of Coastal Engineering*, JSCE, 49, 881-885 (in Japanese).

Tonkin, S., H. Yeh, F. Kato, and S. Sato. 2003. Tsunami scour around a cylinder, *Journal of Fluid Mechanics*, 496, 165-192.

Yamamoto, T. 1977. Wave induced instability in seabeds, *Proceeding of Coastal Sediments '77*, ASCE, 898-913.